In situ diffuse scattering of neutrons in alloys and application to phase diagram determination

R. Caudron, M. Sarfati, M. Barrachin, A. Finel, F. Ducastelle, F. Solal

Classification
Physics Abstracts
64.60C — 61.55H

In situ diffuse scattering of neutrons in alloys and application to phase diagram determination

R. Caudron ([1,2]), M. Sarfati ([1,2]), M. Barrachin ([1,2]), A. Finel ([1]), F. Ducastelle ([1]) and F. Solal ([1,2,3])

([1]) ONERA, B.P. 72, 92322 Châtillon Cedex, France
([2]) Laboratoire Léon Brillouin, CEN Saclay, 91191 Gif sur Yvette Cedex, France
([3]) *Present address :* Laboratoire de Spectroscopie du Solide, Université de Rennes, 35042 Rennes Cedex, France

(*Received 4 February 1992, accepted in final form 6 March 1992*)

Résumé. — Nous avons effectué des mesures de diffusion diffuse de neutrons à différentes températures sur des monocristaux de Pd_3V, Ni_3V, Ni_2V, Ni_3Cr et Ni_2Cr. Nous avons traité les données par moindres carrés, afin d'en extraire les paramètres d'ordre à courte distance. De ces derniers, nous avons déduit des interactions de paires effectives jusqu'au quatrième voisin, par une méthode de CVM inverse. La méthode de moindres carrés est détaillée, ainsi que l'approximation CVM. Le comportement des interactions prévu par les calculs de structure électronique correspondent globalement à nos résultats. Ces derniers nous ont permis de déduire les stabilités de phases et les températures de transition des composés mesurés. Pour les composés de structure DO_{22}, le modèle à quatre interactions rend bien compte de la situation expérimentale. Il n'en est pas de même pour les composés de type Pt_2Mo, où le neuvième voisin (330) joue un rôle important, ainsi que, peut-être, le triplet linéaire dans la direction $\langle 110 \rangle$.

Abstract. — *In situ* diffuse scattering of neutrons has been performed at various temperatures on Pd_3V, Ni_3V, Ni_2V, Ni_3Cr and Ni_2Cr single crystals. The experimental data have been least squares fitted, in order to obtain short range order parameters, from which effective pairwise interactions were deduced up to the fourth neighbour. The least squares procedure is explained, together with the inverse CVM method used to extract interactions from the short range order parameters. We describe the CVM, which approximates the Ising model linking the order parameters to the interactions and the temperature. The trends of the interactions predicted by the electronic structure calculations fit generally with the experimental results. Phase stability and transition temperatures have been deduced from our results : for the DO_{22} structure, they are in agreement with the experimental situation ; for the Pt_2Mo-type structure, the role of the ninth neighbour interaction (330) has been shown to be crucial. We also suspect other interactions, as the triplet in the $\langle 110 \rangle$ direction, to be important for this structure.

1. Introduction.

The study of many phase diagrams relies on the phase stability of substitutional alloys. In the cases of clustering or superstructures of a given parent lattice, statistical mechanics methods

are used, which assume that the internal energy can be expressed as a rapidly convergent sum of pair and higher order multiplet interactions between the atomic species :

$$H = \sum V_{mn}(p_m - c)(p_n - c) + V_{\ell mn}(p_\ell - c)(p_m - c)(p_n - c) + \cdot \quad (1)$$

where c is the concentration and p_n are occupation numbers taking the values 0 or 1 depending on the species at sites n.

In this framework, phase diagrams should be deducible from these interactions, along with other properties, such as antiphase boundaries, core structures of the dislocations in ordered compounds, etc.

A theoretical method to estimate the effective interactions, the inverse method, also called the Connolly-Williams method, relies on band calculations of the ground state energy for a series of ordered structures. The calculated energy for each compound is then expressed as a sum of the effective interactions weighted by the known correlation functions of the compound. A linear system of equations is obtained, and its inversion yields the interactions. In this method, the choice of the significant clusters is rather arbitrary and the interactions are not allowed to vary with the concentration, except through the volume variation.

On the contrary, the General Perturbation Method [1, 2] leads to qualitative arguments enabling, in particular for transition metals alloys, to select the strongest interactions. This method is founded on a perturbation development of the order energy, the reference state, namely the random alloy, being calculated within the CPA (Coherent Potential Approximation). For alloys of normal metals, it legitimates expansion (1). For transition alloys, this procedure, within the Tight Binding Approximation, leads to simple and general results :

— The pair interactions are dominant *versus* the other multiplet interactions, i.e. the order energy can be written :

$$H = \sum{}' J_{mn}\, \sigma_m\, \sigma_n + h \sum \sigma_n \quad (2)$$

where the σ's, related to the p's by $p = (1 - \sigma)/2$, are spin-like operators, taking -1 or 1 values, the J's are the corresponding effective pairwise interactions and h is the chemical potential difference.

— The interactions between the second, third and fourth neighbours are of the same order of magnitude, and generally small compared to the first neighbour interaction. Further interactions are still smaller. This hierarchy is governed by the number of first neighbour $\langle 110 \rangle$ jumps needed to connect the origin to the neighbour under consideration, with an advantage to the straight paths ($\langle 220 \rangle$ fourth neighbours for instance).

This paper is the partial fulfillment of a systematic program whose purpose is to obtain experimental estimates of the effective interactions, in order to compare them with the calculated orders of magnitude and trends and, ultimately, to build phase diagrams. Such estimates could be deduced from the stability of a given compound, but, in this way, only ranges for the interactions can be obtained, because of the discrete nature ($p = 0$ or 1) of the occupation operators in the ordered state. However, in the disordered state, this constraint is lifted and, through an adequate thermodynamical treatment, the measurement of the correlations (short range order parameters) gives a direct access to the effective interactions, with an accuracy limited only to the experimental error bars.

The diffuse scattering of electrons, X-rays or neutrons yields directly the Fourier transform of the pair correlation functions. However, except in favourable cases where the high temperature disordered state can be retained by quench, experiments should be carried out at high temperatures : this rules out X-rays or electrons because, in these methods, the inelastic

scattering, which is very strong at high temperatures, cannot be separated out, and also because the low penetration depth of X-rays or electrons gives a too important weight to the surface, which easily gets contaminated or perturbed.

In the course of the paper, we successively present :

— the criteria used to choose the alloys we have studied ;

— the experimental procedure, with a description of the spectrometer specially built for our studies ;

— the data reduction procedure, which extracts the short range order parameters from the experimental data. It includes the least squares fitting with its error propagation, and the model on which it is based, which takes into account the contribution of the lattice distortions to the scattered intensity ;

— the data analysis, which deduces the effective interactions from the short range order parameters ;

— the discussion, where our measured interactions are compared with those calculated by electronic structure models, and where they are used to predict the stability and the transformation temperatures of the compounds studied. Those properties are compared with experiment ;

— some brief conclusions.

2. Systems studied.

We chose the Pd-V, Ni-V and Ni-Cr systems. The criteria of our choice, selected in order to simplify the reduction and the interpretation of the data, were as follows :

— Binary systems, in order to obtain directly the pair correlation functions from a single experiment.

— Alloys of transition metals because, in this case, the shorter range of the effective interactions leaves less parameters to handle and also because the comparison is more straightforward with the electronic structure calculations developed in our laboratory, which rely on the tight binding method, better suited to describe the transition metals and alloys.

— Non-magnetic alloys, in order to avoid paramagnetic scattering and complications due to the interplay of magnetic and chemical interactions, although those aspects have been treated successfully [3].

— Systems exhibiting many ordered compounds based on the same underlying lattice as the disordered phase : this ensures that the interactions are strong enough. However, too strong interactions must be avoided, in order to leave a large enough temperature range between the disordering temperature and the melting point. The phase diagrams of our systems exhibit three ordered phases based on the FCC disordered lattice : Ni_8V-type, DO_{22}, and Pt_2Mo-type. The Ni_4Mo compound, which occurs in a similar system [4], pertains to the same 1 1/2 0 family as DO_{22} and Pt_2Mo. The structures corresponding to the concentrations we have studied are shown in figures 1a and 1b. These compounds undergo a first order transition towards the disordered phase. The Pt_2Mo-like structure is present in the three systems : Ni_2V, Pd_2V and Ni_2Cr disorder at 920 [5], 970 [6] and 580 °C [7] respectively and their melting points lie around 1 300 °C. The two DO_{22} compounds Ni_3V and Pd_3V disorder at 1 045 [5] and 815 °C [8], and both melt around 1 300 °C. Ni_3Cr is not known to order, probably because its transition temperature is so low that the diffusion is not active enough to let the order set in. Ni_8V, which orders around 400 °C [5], is the only observed compound at this stœchiometry for the systems we have studied.

— Size effect as small as possible : the local distortions are then small, and their contribution to the intensity can be estimated, and corrected, through a first order expansion

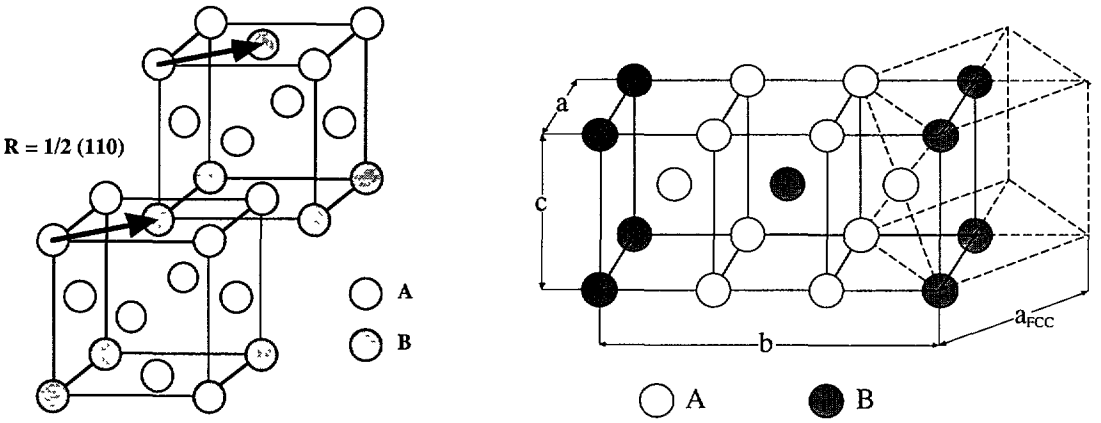

Fig. 1. — a) The DO_{22} structure : the arrows show the periodic antiphase displacements along $\langle 1/2\ 12/0\rangle$ transforming the $L1_2$ into the DO_{22} structure. b) The Pt_2Mo-like structure (solid lines) : the dashed lines represent the underlying FCC structure.

of an exponential function of the lattice displacements. The atomic volumes of V, Cr, Ni and Pd are respectively 13.9, 12.0, 10.9 and 14.7 Å^3 · a maximum lattice mismatch of 8 % occurs for the Ni-V system.

— A sufficient contrast between the components of the alloy : the useful signal is the Laue intensity $4\,\pi c(1-c)(b_A - b_B)^2$ (c : concentration, b's : diffusion lengths of the elements), which is modulated by the distortion and the short range order. This Laue intensity must be sufficient compared to the incoherent scattering cross section, which is a weighted average of the component values. The neutron scattering data for the components of our systems are displayed in table I [9, 10]. The properties displayed in table II were deduced for the specific alloys we have studied, i.e. Ni_2V, Ni_2Cr, Ni_3V, Ni_3Cr and Pd_3V, together with those of vanadium which, because of its isotropic scattering, is the reference element for our experiments. The maximum value of the ratio of incoherent to Laue scattering occurs for Ni_3Cr. It amounts to 4.12 which is not too strong a value.

Previous work has already been performed on the Ni-Cr system, for which the alloys are easy to quench (the Ni_2Cr phase does not order easily [7]). Schweika *et al.* [11] and Schönfeld *et al.* [12] carried out measurements similar to ours on quenched single crystals containing 11 and 20 at.% Cr respectively. An experiment was performed by Vintaykin [13] on a Ni_2Cr sample annealed at 500 °C, i.e. out of equilibrium as $T_c = 580$ °C. Except our own preliminary publications, no work has yet been reported on Ni-V and Pd-V systems.

Table I. — *Neutron data for the elements.*

	V	Cr	Pd	Ni
Scattering length b (10^{-12} cm)	− 0.04	0.35	0.60	1.03
$\sigma^{\text{incoherent}}$(barns)	4.78	1.83	0.09	4.8
σ true absorption (barns)	6.74	4.32	9.6	6.48

Table II. — *Neutron data for the alloys studied.*

	V	Pd_3V	Ni_3V	Ni_2V	Ni_3Cr	Ni_2Cr
$\sigma^{\text{incoherent}}$(barns)	4.78	1.263	4.79	4.79	4.14	3.92
Absorption coef. μ (cm^{-1})	0.85	0.35	1.23	1.26	0.90	0.86
Laue $4\pi c_A c_B (b_A - b_B)^2$ (barns)	—	0.96	2.74	3.14	1.115	1.341
$I^{\text{incoherent + Mult. Scatt.}}$ (Laue units)	—	1.58	1.77	2.20	4.12	3.26

We attempted twice to perform an experiment on Pd_2V, but the single crystals, which were perfect in the disordered state at room temperature, became polycrystalline upon heating. This phenomenon was explained by strains and small twins quenched in the sample : during heating, under the influence of the strains, the twins are developed in the form of thermal twins which destroy the single crystal structure [14].

3. Experimental.

3.1 SPECTROMETER. — Faced to our experimental needs, we were led to build a neutron spectrometer dedicated to the *in situ* diffuse scattering of metallic alloys at high temperatures. This work was performed together with the team of de Novion (Laboratoire des Solides Irradiés ([1])). The instrument is located on a cold neutron guide at the Laboratoire Léon Brillouin. It is shown schematically in figure 2.

To collect as much information as possible, we avoided the powder method, which washes out the intrinsic anisotropy of the problem : in our instrument, the sample can be rotated accurately around its vertical axis, in order to perform experiments on single crystals.

The 2-axis geometry, with a multidetector rather than a position sensitive detector, and an energy analysis performed by a chopper (3) and a time of flight, has been preferred to a 3-axis for the following reasons :

— The counting rate increase due to the multidetector overcompensates the loss of intensity due to the chopper : the transmission of the chopper, whose slits are adjustable, is generally around 10 % and the spectrometer is equipped with 48 ^{3}He detectors (6), spaced every 2.5°, at 1.5 m of the sample.

— With the 2-axis layout, the sample geometry is better defined and it is possible to rotate the sample without moving the furnace : the background and absorption corrections are easier and safer.

— A major drawback of the 2-axis geometry is that it gives access only to planes of the reciprocal space passing through the origin, whereas, with a 3-axis spectrometer, any point can be reached. However, the exploration of two planes of high symmetry treated with a least squares fit has been shown [15] to be equivalent to a 3-dimensional scan processed by the Sparks and Borie method [16].

The diffuse scattering due to chemical short range order is periodic in the reciprocal space : this enables us to separate it from the non-periodic intensity due to the distortions induced by

([1]) CEA/CEREM/DTM/SESI, Ecole Polytechnique, 91128 Palaiseau Cedex, France.

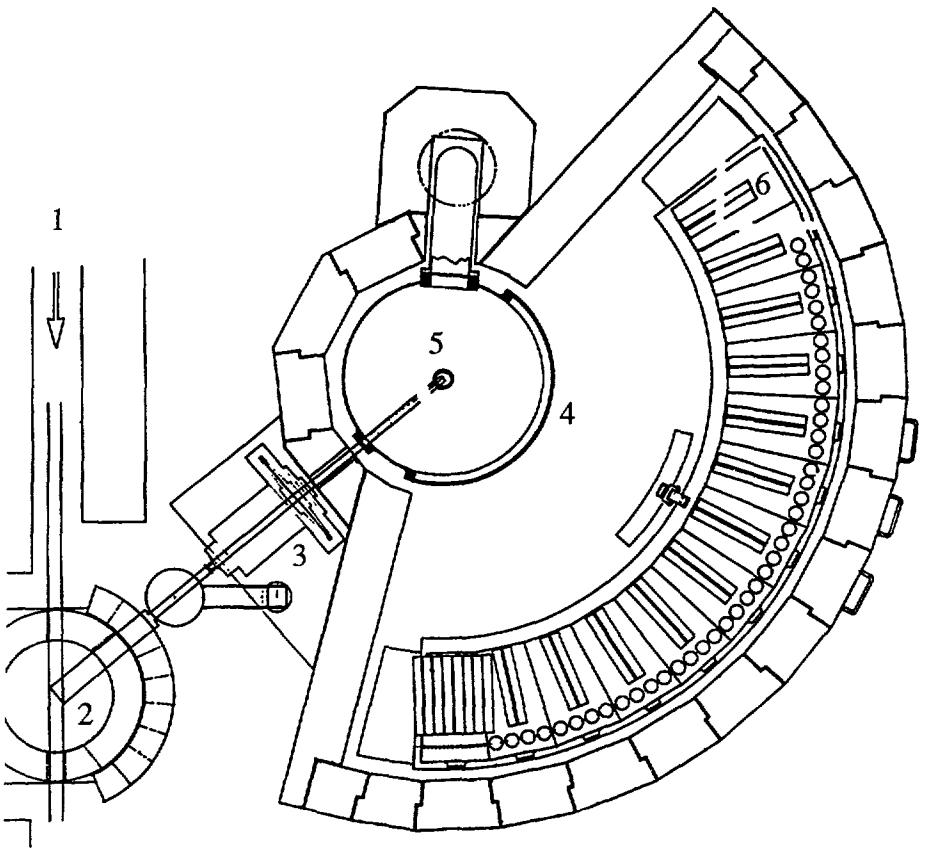

Fig. 2. — The spectrometer designed for *in situ* diffuse scattering of neutrons. 1 : Neutron guide ; 2 : 002 Pyrolitic graphite monochromator ; 3 : Chopper ; 4 : Vacuum vessel (0.8 Meter diameter) ; 5 : Furnace resistor (Nb 0.1 mm thick, 30 mm diameter) ; 6 : ^{3}He filled detectors.

the different sizes of the atoms. Therefore, the explored range must include at least the second Brillouin zone and a short enough incident wavelength is needed : in our instrument, it can be continuously varied from 5.9 to 2.6 Å. At 2.6 Å, which is the most frequently used wavelength, the wavelength accuracy is $\delta\lambda/\lambda \sim 10^{-4}$ and the flux on the sample is 3×10^6 n/cm^2 without chopper. With the usual setting of the chopper, the flux is reduced to 3×10^5 and the energy resolution is about 5 and 3 meV for phonon annihilation and creation, respectively.

The sample is located at the center of an evacuated stainless steel vessel (4), in order to minimize the stray scattering by air. The diameter of this vessel is 80 cm, so that the neutrons scattered by the entrance window cannot reach the detectors if they are properly collimated. Thanks to these features, the background is reduced down to 100 counts per hour and per detector.

The furnace resistor (5), 30 mm in diameter, is made of a 0.1 mm thick foil of niobium. A 100 mm diameter screen, made of the same Nb foil, enables us to reach 1 300 °C without injecting too strong a current through the resistor.

3.2 SAMPLE PREPARATION. — Single crystal rods of random orientation were grown by the Bridgeman method, by J. L. Raffestin (ONERA) and by R. Rafel (CNRS Grenoble,

Cristaltech). If the length of the as-grown crystal was sufficient, two cylinders were spark cut, with their axis along ⟨100⟩ and ⟨110⟩ (or ⟨111⟩), and placed vertically in the spectrometer. If the crystal was too short, one cylinder only was cut, with its axis along a direction halfway between ⟨100⟩ and ⟨110⟩ ; in the spectrometer, it was tilted by 22.5° towards one or the opposite direction to scan the ⟨100⟩ or ⟨110⟩ plane. The various sizes and tilt angles of the samples are given in table III. The samples were checked by the neutron Laue method, to ensure that they were single crystals. Their orientations were adjusted to an accuracy of ± 1° by the X-ray Laue method. Their concentrations were measured by electron microprobe : table III also displays the results of the analysis.

Table III. — *Characteristics of the samples used : diameter, height, tilt angle and concentration.*

	Pd_3V		Ni_3V		Ni_2V		Ni_3Cr		Ni_2Cr	
Planes	100	110	100	110	100	111	100	110	100	110
Diameter (mm)	8		6		10	8	5		6.5	
Height (mm)	16		10		35	9	6		10	
Tilt angle (deg.)	0	45	0	0	0	0	0	0	24	21
V or Cr content	25		25		32		26		36	

4. Data reduction.

4.1 ELASTIC SELECTION. — At the temperatures corresponding to the disordered state of our samples, strong phonon annihilation processes occur, and an energy analysis in necessary to reject the corresponding intensity. This is performed by a time-of-flight system. A typical time-of-flight spectrum is shown in figure 3. As a consequence of the long incident wave

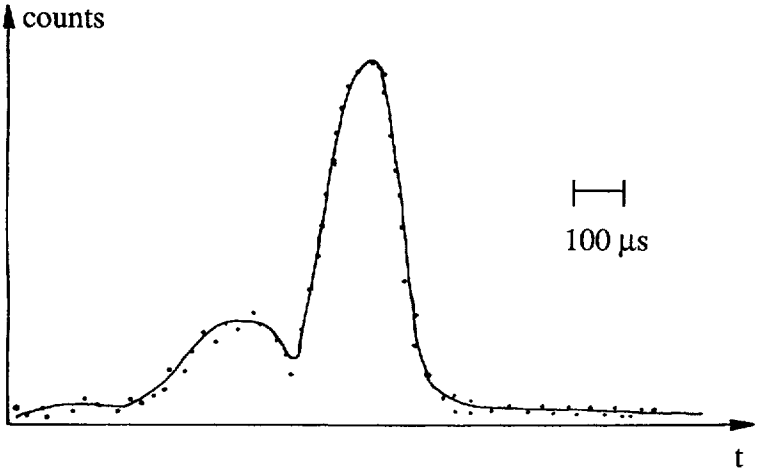

Fig. 3. — Time of flight spectrum.

length, there is no phonon creation, except at the close vicinity of the Bragg peaks : the right, low energy, sides of the spectra retain the trapezoidal shape typical of the incoming burst. We integrate the spectra from the right side until they deviate from this shape, and we use the symmetry to restitute the remaining data.

4.2 CORRECTIONS AND CALIBRATIONS. — The scattering cross sections were deduced from the integrated time of flight spectra, after standard corrections, i.e. :

— The instrumental background I_s^b was subtracted from the measured intensity I_s. It is given by :

$$I_s^b = I_{BN} + T_S(0)(I_E - I_{BN}) ,$$

where I_E denotes the intensity without sample (empty furnace) : about 100 counts per hour and per detector, I_{BN} is the intensity measured on a piece of boron nitride having the same shape as the sample : the same order of magnitude as I_E, $T_S(0)$ is the transmission coefficient of the sample in the direction of the unscattered beam ($2\theta = 0$).

— The data were corrected for absorption by a linear interpolation of the table published by [9] for cylindrical samples. This table displays, for a given value of the diffraction angle 2θ, the transmission coefficient $T(2\theta)$, calculated by an averaging of the absorption along all possible paths in the circular section of the sample by the scattering plane. To evaluate the linear absorption coefficients needed for these calculations, the Laue and incoherent cross sections were added to the true absorption cross section. The calculated values are displayed in table II. The maximum error induced by the cylindrical approximation is about 5 % for the most tilted sample (Ni_2Cr, 24°, 6.4 mm diameter).

— The incoherent scattering σ^{inc}, displayed in table II, was subtracted from the measurements, together with the multiple scattering σ^{MS}, estimated by the Blech and Averbach method [17].

— The value of B entering the Debye-Waller correction $\exp(B|q|^2)$, with $|q| = 4\pi \sin\theta/\lambda$, can be estimated from the elastic constants of the alloys, through a harmonic Debye model. However, this model is unrealistic because strong anharmonic processes occur at the high temperatures of our experiments : B was left as an adjustable parameter B_0 in the least squares procedure described below.

— The calibration relies on the scattering, at room temperature, by a vanadium standard of the same shape as the sample, corrected similarly for background and absorption, but with a fixed Debye-Waller coefficient $B_v = 0.0036$ Å^2 [18]. The neutron data used for vanadium are displayed in table II. The final formula was, in units of the sample Laue scattering σ_s^{Laue} .

$$\frac{d\sigma}{d\Omega} = \frac{I_s - I_s^b}{I_v - I_v^b} \frac{T_v(\theta)\, N_v(\sigma_v^{inc} + \sigma_v^{MS}) \exp(-B_v|q|^2)}{T_s(\theta)\, N_s\, \sigma_s^{Laue} \exp(-B_0|q|^2)} - \sigma_s^{inc} - \sigma_s^{MS} \qquad (3)$$

Most of the symbols in this formula have been defined before, the lower indices s and v refer to the sample and to the vanadium standard, respectively ; I_v^b is the intensity measured without sample at room temperature, as for the vanadium standard. σ_s^{inc} and σ_s^{MS} are evaluated in Laue units. The error on an experimental counting I_s, calculated on grounds of Poissonian errors, is given by :

$$(1 + \sigma_s^{inc} + \sigma_s^{MS}) \sqrt{\frac{I_s + I_s^b}{(I_s - I_s^b)^2} + \frac{I_v + I_v^b}{(I_v - I_v^b)^2}} . \qquad (4)$$

4.3 CORRECTED RESULTS. — Examples of the corrected maps are shown in figures 4a and b. Except in the neighbourhood of the Bragg points, their symmetries are very close to those of the reciprocal lattice of the FCC lattice : the smallness of the deviations show that the distortion effects are not too strong. Because of the imperfections of the elastic selection, the Bragg peaks are strongly broadened, and elongated along directions which do not agree with the other symmetries of the maps : the symmetry of the phonon branches, which should be consistent with those of the reciprocal lattice, is broken by the scattering geometry.

The maxima showing up in the ⟨110⟩ or ⟨111⟩ planes correspond to saddle points in the ⟨100⟩ planes, situated on the 110 lines.

The intensities should be identical along the 100 and 110 lines, which are common to the ⟨100⟩ and ⟨110⟩ maps (only the 110 line is common to the ⟨100⟩ and ⟨111⟩ planes) : discrepancies reaching 4 % of the total intensity for Ni_3Cr (incoherent scattering included) can be explained by the small size of the samples, which cannot be accurately aligned in the beam. Before the fit, correcting factors F_c were applied to the ⟨110⟩ or ⟨111⟩ data, in order to compensate these discrepancies.

4.4 MODEL. — Throughout the paper, the Relative Lattice Units (RLU) [19] will designate the coordinates h_1, h_2, h_3 of the scattering vector $\mathbf{q} = 2\pi(\mathbf{b}_1 h_1 + \mathbf{b}_2 h_2 + \mathbf{b}_3 h_3)$, where the $\mathbf{b}$'s are the unit vectors of the reciprocal space (e.g. $\mathbf{b}_1 = \dfrac{\mathbf{a}_2 x \mathbf{a}_3}{\mathbf{a}_1 \cdot (\mathbf{a}_2 x \mathbf{a}_3)}$, where the

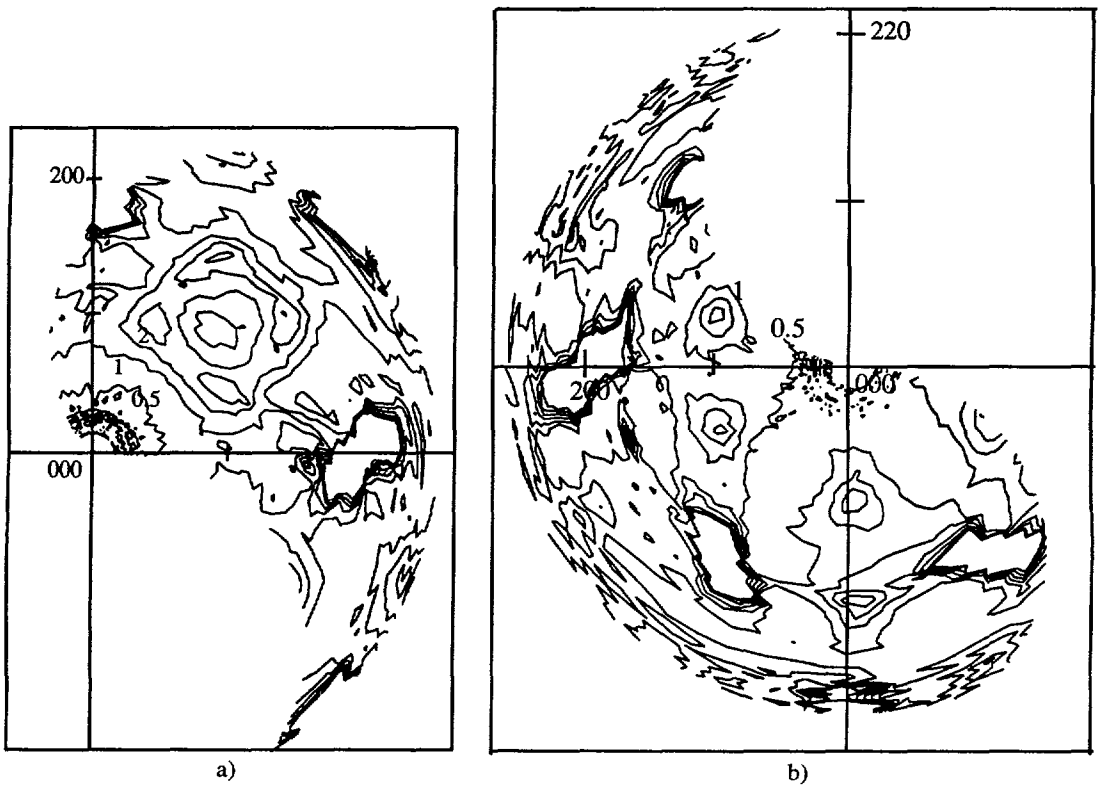

Fig. 4. — a) Map of the as measured diffuse intensities in the ⟨100⟩ plane for Ni_3Cr at 560 °C. Laue units. b) Map of the as measured diffuse intensities in the ⟨110⟩ plane for Ni_3Cr at 560 °C. Laue units.

a's are the edges of the FCC unit cell). The following formalism can be found in reference [20].

The general expression for the intensity scattered by binary alloys at the scattering vector **q** is :

$$I(\mathbf{q}) = \sum_{i=1}^{N} \sum_{j=1}^{N} b_i\, b_j \exp[i\mathbf{q}(\mathbf{R}_i - \mathbf{R}_j + \boldsymbol{\delta}_i - \boldsymbol{\delta}_j)]$$

where : $\mathbf{R}_i$ is the position of the i-th site, b_i and b_j are the scattering factors for the atoms i and j, $\boldsymbol{\delta}_i$ and $\boldsymbol{\delta}_j$ are the displacement vectors from the lattice position to the true atom position. The sums run on the sites of the FCC lattice.

If the $\boldsymbol{\delta}_{ij} = \boldsymbol{\delta}_i - \boldsymbol{\delta}_j$ are small, the exponential can be expanded to first order and the scattered intensity is split into two additive terms, due respectively to the short range order and to the lattice distortions :

$$I_1(\mathbf{q}) = \sum_{i=1}^{N} \sum_{j=1}^{N} b_i\, b_j \exp[i\mathbf{q}(\mathbf{R}_i - \mathbf{R}_j)]$$

and

$$I_2(\mathbf{q}) = \sum_{i=1}^{N} \sum_{j=1}^{N} i\mathbf{q} \cdot \boldsymbol{\delta}_{ij}\, b_i\, b_j \exp[i\mathbf{q}(\mathbf{R}_i - \mathbf{R}_j)] .$$

After separation of the Bragg scattering and thermodynamic averaging, the first term becomes the standard expression for the intensity due solely to the short range order :

$$I_1(\mathbf{q}) = I_{\text{Laue}} \sum_{n=0}^{N} \alpha(\mathbf{R}_n) \exp(i\mathbf{q}\mathbf{R}_n) \tag{5}$$

where the $\alpha(\mathbf{R}_n)$ stand for the usual Warren-Cowley short-range order parameters [21]. This expression is periodic in reciprocal space and linear in the α's.

The second term can be evaluated by taking into account the cubic symmetry of the problem :

$$I_2(\mathbf{q}) = -Nc_A\, c_B (b_A - b_B)^2 \sum_{\ell, m, n} (h_1\, \gamma^X_{\ell mn} + h_2\, \gamma^Y_{\ell mn} + h_3\, \gamma^Z_{\ell mn}) \sin 2\pi(h_1 \ell + h_2 m + h_3 n) \tag{6}$$

where ℓ, m, n stand for the coordinates of the vector $\mathbf{R}_i - \mathbf{R}_j$ joining two sites.

This intensity is not a periodic function of **q**, as it is a linear combination of the components h_1, h_2, h_3 of **q** with periodic coefficients. It is linear in the distortion parameters :

$$\gamma_{\ell mn} = \frac{2\pi}{b_A - b_B} \left[\left(\frac{c_A}{c_B} - \alpha_{\ell mn} \right) \langle x^{AA}_{\ell mn} \rangle\, b_A - \left(\frac{c_B}{c_A} - \alpha_{\ell mn} \right) \langle x^{BB}_{\ell mn} \rangle\, b_B \right] \tag{7}$$

where, for instance $\langle x^{AA}_{\ell mn} \rangle$ is the averaged x component of the displacements $\boldsymbol{\delta}_{ij}$ between two A atoms. This expression has been derived from a more complicated one involving also the average displacements between unlike species $\langle \boldsymbol{\delta}^{AB}_{ij} \rangle$. The latter quantity has been eliminated by noticing the existence of an average lattice [22].

A third term is added by the adjustment procedure for the Debye-Waller factor $\exp(-B|\mathbf{q}|^2)$: the exponential is developed as $(1 - \Delta B|\mathbf{q}|^2) \cdot \exp(-B_0|\mathbf{q}|^2)$, B_0 being a trial value adjusted to obtain a small ΔB. The data are divided by the second factor before the least squares procedure. $I(\mathbf{q})$ is still multiplied by $(1 - \Delta B|\mathbf{q}|^2)$. This factor is converted into

an additive contribution $-I(\mathbf{q})\,\Delta B\,|\mathbf{q}|^2$, which is linear in ΔB and can therefore be included in the multilinear least squares fit providing the short-range order and distortion parameters. If not small, the values for ΔB can be added to B_0, and the fit can be iterated until ΔB is really small.

4.5 SELECTION OF THE RELEVANT DATA. — Some data must be discarded, because they are polluted by quasi-elastic scattering. This circumstance, together with the scanning of only two unequivalent planes passing through the origin, removes us from the ideal sampling of the reciprocal space, which would be an evenly spaced three dimensional mesh. The criteria of our choices rely on the comparison between the experimental maps and the intensity function reconstructed using relations (5) and (6), with the parameters α and γ supplied by the fit.

Around the origin, the phonon intensity is negligible, and the data are valid down to 0.3 $Å^{-1}$ or 0.17 RLU [19], a reasonably low limit due to the extension of unscattered beam. These data are important because, even in the absence of distortion, no equivalent points can be reached using the reciprocal space periodicity : in the vicinity of the Bragg peaks, many data points are spoiled by quasi-elastic scattering.

Around the Bragg points, a simple way to discard unrelevant data points would be to keep only those whose distance from the Bragg positions is longer than some radius R_c. Because of the strongly asymmetric broadening of the Bragg peaks, R_c must be adjusted to the huge value of 1.16 $Å^{-1}$ or 0.65 RLU, so that some 600 experimental points are eliminated, on a total of about 4 000. The distortion parameters are then allowed to take too strong values and the reconstructed intensity oscillates, leading to unphysical (negative) values in the regions where too many data have been suppressed. This behaviour is induced by the elimination of a lot of valid data, which would be useful, as their comparison with those collected around the origin contributes to the distortion parameters. To avoid these difficulties, we recover the points contained in the circles of radius R_c if their intensity is lower than a threshold value I_c . if I_c is chosen too low, the points kept in the circles are too scarce, and unphysical oscillations of the reconstructed intensity occur ; if I_c is too high, the wings of the broadened Bragg peaks are selected and the reconstructed maps exhibit an anomalously steep increase around the origin and the Bragg positions. With this procedure, some 400 data points were recovered among the 600 excluded points in the 0.65 RLU circles centered around the Bragg peaks.

4.6 LINEAR LEAST SQUARES PROCEDURE. — The data were fitted using a multilinear least squares routine based on the singular value decomposition [23]. Let I_q ($q = 1 \ldots Q$, Q = number of experimental points) be the vector of the measured intensities. The problem is to determine the vector β_r of the parameters (altogether short range order, incoherent scattering, distortion and linearized Debye-Waller correction) ($r = 1 \ldots R$ = number of unknown parameters, $\ll Q$), the intensity being given in terms of the parameters by $I_q \cong M\beta_r$. This relation is to be solved in the sense of least squares. The known rectangular matrix $M(Q, R)$ is made of Q lines and R columns.

To obtain the decomposition in singular values, the following double unitary transformation is made, using the unitary matrices $u(Q, Q)$ and $w(R, R)$: $\lambda_i = u\tilde{I}_q$; $\beta_r = w\tilde{\beta}_r$ and $M = uXw^+$ The relation $I_q \cong M\beta_r$ is replaced by $I_q \cong X\beta_r$, $X(Q, R)$ taking the form : $M = \begin{bmatrix} D \\ 0 \end{bmatrix}$, where all the elements of the sub-block 0 ($Q - R$, R) are zeros, and the remaining sub-block $D(R, R)$ is diagonal, its elements being the singular values λ_i.

The routine supplies the singular values and the matrices u and w. The problem is solved by

first calculating $\tilde{I}_q = u^+ I_q$. The elements of $\tilde{I}_q$ are then multiplied by the inverse singular values λ_i^{-1} to obtain the elements of $\tilde{\beta}_r$, and finally w is applied.

This method is equivalent to a standard least squares method, but it is more efficient and, moreover, it gives access to the error bars : as the intensity is nearly constant because of the strong incoherent component, the uncertainity volume on the vector I_q can be assumed to be a hypersphere of radius δI_q whose order of magnitude is given by (4) ; the unitary transformation u does not change this volume which, in the $\tilde{I}_q$ space, can be assimilated to a hypercube ; the multiplication by λ_i^{-1} stretches it into a known « brick », and the transformation w is easily applied to obtain the error in the β_r space. The error on the i-th parameter can be written :

$$\delta\beta_r^i = \delta I_q \sum_{j=1}^{R} (w_{ij}/\lambda_j) .$$

With a Gaussian superposition of errors, we obtain :

$$\delta\beta_r^i = \delta I_q \sqrt{\sum_{j=1}^{R} (w_{ij}/\lambda_j)^2} .$$

The routine also supplies the residual

$$\sum = \sqrt{\frac{\sum_{q=1}^{Q} (I_q - I_q^{\text{calc}})^2}{Q - R}} \tag{8}$$

which is given in table IV and is to be compared with the error for the individual data points (4), generally around 0.1.

4.7 DISTORTIONS AND SHORT RANGE ORDER PARAMETERS. — The ⟨100⟩ and ⟨110⟩ or ⟨111⟩ planes were fitted together. The number of short-range order and distortion parameters was increased until the introduction of further parameters did not modify the previous ones. The short-range order parameters are displayed in table IV, with their error bars, for all alloys at all temperatures. This table also displays the residual $\sum$ given by (8), the final Debye-Waller coefficient B and the correcting factor F_c mentioned in section 4.3, needed to compensate the discrepancies between the ⟨100⟩ plane and the other planes. The distortion parameters are shown in table V, only for Ni_2V at 955 °C, for which they are the strongest. Examples of maps reconstructed with these parameters are shown in figures 5a and b : they faithfully reproduce the raw data of figures 4a and b.

As expected, for a given alloy, the order parameters decrease with increasing temperature.

The parameter α_0 should be equal to unity because it represents the scattering averaged in the first Brillouin zone. The discrepancies happen to be large, especially for Ni_2V and Ni_3Cr. The latter sample is tiny, and a small misalignment can attenuate significantly the signal. This explanation is not valid for the other samples. The Ni_2Cr behaviour seems correct, but the discrepancies for Ni_2V remain to be explained.

Table V shows that the lattice distortion parameters for Ni_2V are generally small. They behave similarly, but they are smaller for all the other alloys we have investigated. The most prominent one is $\gamma_{002} = -0.03$. Using formula (7) and noticing that the γ's are mostly sensitive to the nickel displacements, we can estimate $\langle x_{002}^{\text{Ni, Ni}} \rangle \sim -2.4 \times 10^{-3}$ times the lattice parameter. The order of magnitude of the Cr-Cr displacements should be similar. The

Table IV. — *Short-range order parameters for shells up to the tenth, extracted from our data. The error bars, in parentheses, concern the latest digit written. The table also displays the least squares distance Σ, which is to be compared to the statistical error (about 0.1), the measured Debye-Waller parameter* B, *in* $(RLU)^{-2}$ [19], *fitted to our data, and the factor* F_c *by which the data for the* ⟨110⟩ *or* ⟨111⟩ *planes has been multiplied in order to fit the data for the* ⟨100⟩ *plane.* * *· for* α_0 *(integrated intensity in the first Brillouin zone), the experimentally measured quantity is not* α_0, *but* $\alpha_0 + \sigma^{inc} + \sigma^{MS}$ *(in Laue units). The displayed value has been normalized by* $1 + \sigma^{inc} + \sigma^{MS}$

lmn	Pd_3V 800 °C	Ni_3V 1 100 °C	Ni_2V 955 °C	Ni_2V 975 °C	Ni_2V 1 070 °C	Ni_2V 1 140 °C	Ni_3Cr 560°	Ni_3Cr 720 °C	Ni_2Cr 650 °C	Ni_2Cr 800 °C
000*	0.985	0.973	0.825	0.827	0.829	0.834	0.951	0.843	0.969	0.935
001	− 0.16(2)	− 0.131(2)	− 0.1217(8)	− 0.1201(8)	− 0.1115(8)	− 0.1045(8)	− 0.0874(5)	− 0.0674(6)	− 0.0997(6)	− 0.080(1)
002	0.17(1)	0.117(2)	0.13(2)	0.12(2)	0.11(1)	0.08(2)	0.0681(7)	0.0475(8)	0.0732(8)	0.051(1)
112	0.01(1)	− 0.040(2)	0.0460(5)	0.0427(5)	0.0367(4)	0.0307(5)	0.0322(4)	0.0186(5)	0.0189(4)	0.0058(7)
022	0.03(1)	− 0.010(2)	− 0.041(2)	− 0.039(2)	− 0.029(7)	− 0.027(1)	− 0.0337(5)	− 0.0238(6)	− 0.0184(5)	− 0.0063(8)
013	− 0.04(1)	− 0.035(1)	− 0.0367(6)	− 0.0372(6)	− 0.0263(6)	− 0.0207(6)	− 0.0134(3)	− 0.0079(3)	− 0.0053(4)	− 0.0038(6)
222	0.00(1)	− 0.0405(5)	− 0.020(1)	− 0.008(1)	− 0.0131(6)	− 0.006(1)	− 0.0186(5)	− 0.0098(6)	− 0.0050(6)	− 0.0042(8)
123	− 0.01(1)	0.085(5)	0.0078(4)	0.0062(4)	0.0048(4)	0.0045(4)	0.0035(2)	0.0007(3)	0.0028(3)	0.0050(4)
004	0.07(1)	0.043(2)	0.00(1)	− 0.02(1)	− 0.001(5)	− 0.04(1)	0.0190(6)	0.0066(8)	0.0077(8)	0.004(1)
033	− 0.01(1)	0.000(1)	0.007(1)	0.009(1)	0.008(1)	0.008(1)	0.0185(4)	0.0114(5)	0.0102(5)	0.0096(7)
114	0.01(1)	0.004(1)	− 0.0028(6)	0.0004(5)	0.0017(5)	0.0027(6)	0.0029(3)	0.0033(3)	− 0.0012(4)	0.0001(6)
Σ	0.26	0.21	0.14	0.15	0.14	0.15	0.22	0.21	0.23	0.23
B	0.056	0.052	0.047	0.057	0.068	0.070	0.029	0.046	0.0697	0.077
F_c	1.000	1.000	1.000	1.000	1.000	1.000	1.000	0.963	1.05	1.05

Table V. — *Lattice distortion parameters for* Ni_2V *at* 955 °C.

ℓmn	$\gamma_{\ell mn}$
101	0.0162(7)
200	− 0.031(2)
112	− 0.0086(5)
211	− 0.0015(6)
202	0.012(1)
103	− 0.0052(7)
301	0.0010(7)
222	0.0080(8)
123	0.0042(4)
213	− 0.0052(5)
312	− 0.0037(4)
400	− 0.008(2)
114	0.0006(4)
303	0.0015(6)
411	− 0.0026(5)

sign of this quantity means that, on the average, two nickel atoms in second neighbour position are closer to one another than the two undisplaced positions of the average lattice : this is consistent with the small size of the nickel atoms compared to the other components of the alloys. The magnitude of this quantity tells us that, as $\mathbf{q}$ is at most 2.5 RLU [19], the product $2\ \pi\mathbf{q} \cdot \boldsymbol{\delta}_{ij}$ is smaller than 0.04, and the expansion leadint to (6) is validated.

The Debye-Waller parameters are stronger than expected from the harmonic theory : this is not surprising, as the anharmonic effects are strong and a static Debye-Waller component may be important.

The ⟨100⟩ maps reconstructed with the short range parameters only are shown in figures 6a, b, c, d and e.

For nearly all the samples, the maxima occur at the 1 1/2 0 special points, located in the ⟨100⟩ planes. The only exception is Pd_3V, for which the maxima occur at the 100 special points. This location is surprising as Pd_3V orders on the DO_{22} structure, which shows superstructure peaks at 1 1/2 0 positions : we will show later on that this contradiction is

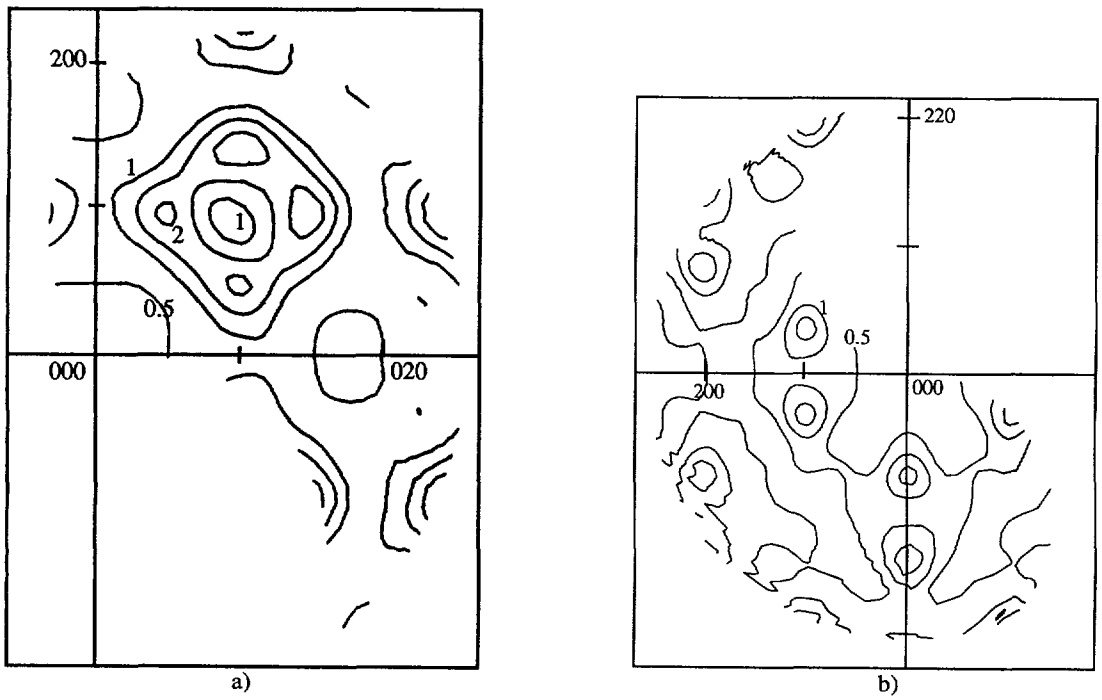

Fig. 5. — a) Map of the diffuse intensities in the ⟨100⟩ plane for Ni_3Cr at 560 °C, reconstructed with the fitted short-range order and distortion parameters. Laue units. b) Map of the diffuse intensities in the ⟨110⟩ plane for Ni_3Cr at 560 °C, reconstructed with the fitted short-range order and distortion parameters. Laue units.

explained by a peculiar set of interactions. The same problem apparently arises for the A_2B composition for which the superstructure peaks show up at the 2/3 2/3 0 positions, but the situation is not the same because, at this composition, no structure can be built with 1 1/2 0 concentration waves.

5. Data analysis : effective interactions.

We have obtained the correlation functions (α's) in the disordered state. Our purpose is to deduce the interactions (J's), which are linked to the (α's) by the Ising Hamiltonian (2). We will first explain the methods to solve (2). But this method will yield the α's as functions of the J's : we will then explain the reversing method used to obtain the J's as functions of the α's and we will explicit the error propagation. The results and some comments will finally be given.

5.1 SOLVING THE ISING HAMILTONIAN : THE CLUSTER VARIATION METHOD. — The CVM is now recognized as one of the most precise techniques for solving the Ising model when no exact solution is available. Since its first derivation by Kikuchi [24], many review articles have been written on the CVM formalism, see e.g. [25, 2]. Hence, we will not give any detail, but rather try to illustrate the basic ideas which underline the theory.

The equilibrium properties at finite temperature are governed by the equilibrium free energy :

$$F = U - TS$$

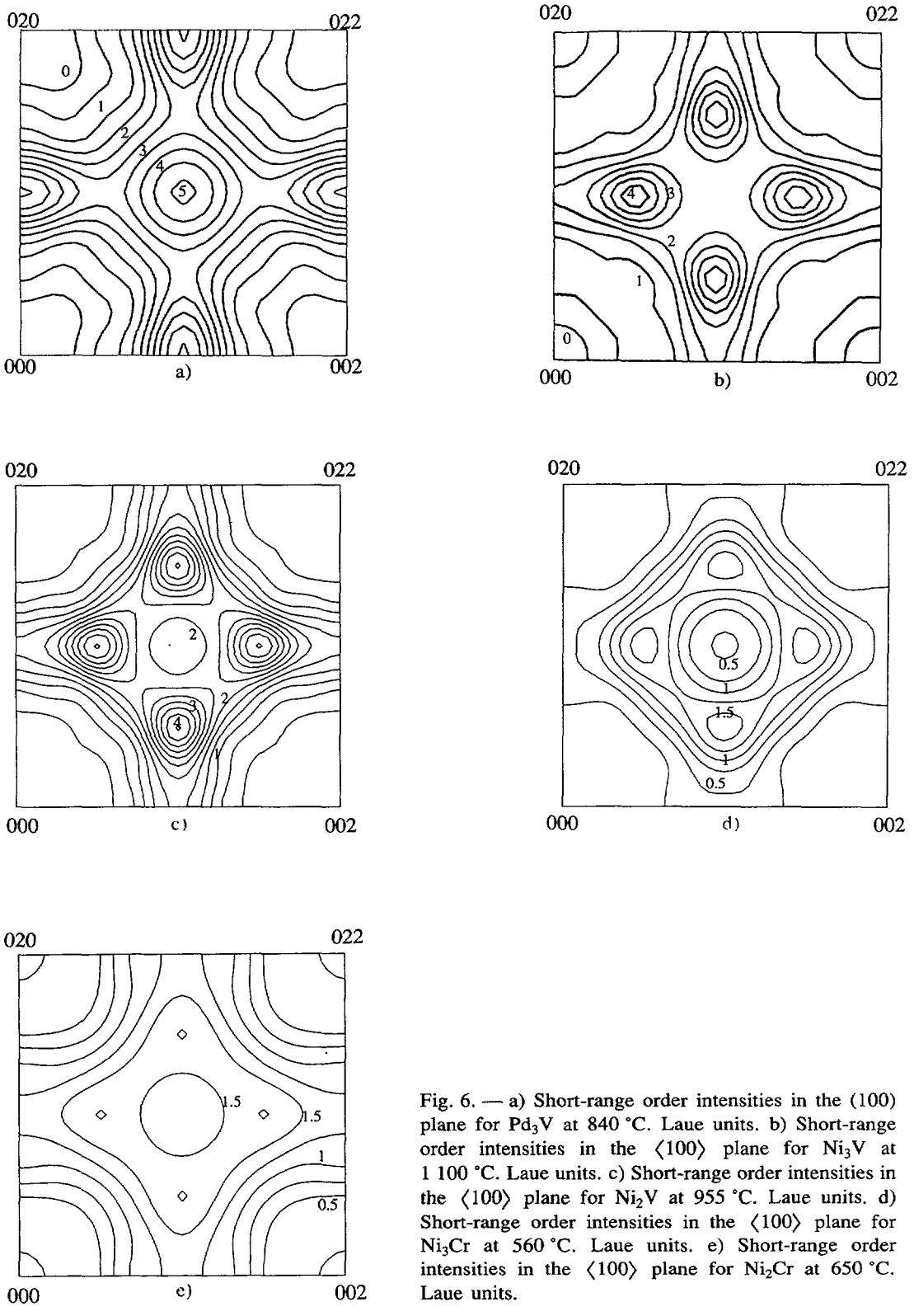

Fig. 6. — a) Short-range order intensities in the (100) plane for Pd_3V at 840 °C. Laue units. b) Short-range order intensities in the ⟨100⟩ plane for Ni_3V at 1 100 °C. Laue units. c) Short-range order intensities in the ⟨100⟩ plane for Ni_2V at 955 °C. Laue units. d) Short-range order intensities in the ⟨100⟩ plane for Ni_3Cr at 560 °C. Laue units. e) Short-range order intensities in the ⟨100⟩ plane for Ni_2Cr at 650 °C. Laue units.

where U, the internal energy, is the thermodynamic average of the Hamiltonian H, and S is the entropy. More precisely :

$$U = \sum_C \rho(C) H(C)$$

$$S = -k \sum_C \rho(C) \operatorname{Log} \rho(C)$$

where $\rho(C)$, the probability of the configuration C, is given by :

$$\rho(C) = \exp(-\beta H(C))/Z ; \quad Z = \sum_C \exp(-\beta H(C)) .$$

Naturally, the problem is that we do not know how to compute $\rho(C)$ in the thermodynamic limit of an infinite system. The basic ingredient of any mean field theory is then to approximate these probabilities.

The well-known Bragg-Williams approximation (or the standard mean-field theory) consists in factorizing $\rho(C)$ on the site probabilities :

$$\rho(C) = \prod_n \rho(\sigma_n)$$

where $\rho(\sigma_n)$ is the probability function of site n. In other words, the total entropy S is replaced by the sum of site entropies. Due to the variational properties of the free energy, the functions $\rho(\sigma_n)$ are subsequently determined through a global minimization of the approximate free energy functional. Obviously, this approach neglects the correlations between site occupancies.

The next approximation consists into re-introducing the pair correlations. More precisely, the probability function $\rho(C)$ is now factorized on the first neighbour pair probabilities :

$$\rho(C) = \prod_{nm} \rho(\sigma_n \sigma_m) / \prod_n \rho^{p-1}(\sigma_n) ,$$

where the denominator has been introduced in order to correct the pair overlap. Indeed, if p is the connectivity of the lattice, each site belongs to p first neighbour pairs and then, in a way, is counted p times in the numerator. This overcounting is suppressed by the denominator and it is easily verified that this factorization scheme is exact in the high temperature limit.

The CVM is just a generalization of the above procedure to any given basic cluster α. For a given choice of α, the approximate probability reads :

$$\rho^{\mathrm{CVM}}(C) = \prod_\beta {}^*\rho_\beta^{a_\beta}$$

where the asterix means that the product runs over the subcluster β included in at least one cluster of type α. As above, the coefficients a_β are determined in such a way that they suppress the overcounting due to the cluster overlap (for the basic cluster α, the coefficient a_α is of course equal to one). The equilibrium free energy is finally obtained by minimizing the CVM functional with respect to the cluster probabilities ρ_α.

Obviously, the quality of the CVM relies on the choice of the basic cluster which can, and must, be adapted to the Hamiltonian of the problem. In the present case, we need pair interactions up to the fourth shell on the FCC lattice. The smallest clusters to be used in such a case are the face-centered cube itself, which contains 14 points, and, simultaneously, the 13-

point cluster formed by one site surrounded by its twelve first neighbours (see Fig. 7). This approximation is referred to as the 13-14-point approximation.

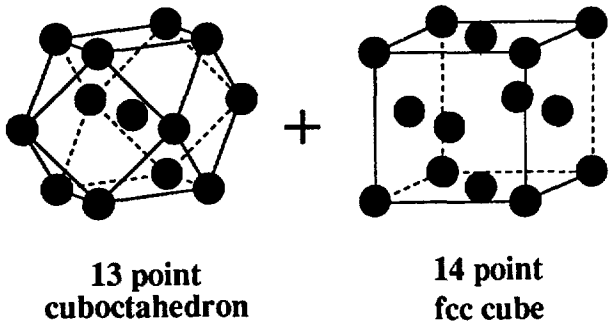

Fig. 7. — Basic cluster used for the CVM approximation.

5.2 REVERSING THE RELATIONSHIP. — Whatever the method used to solve the Ising Hamiltonian (2), the α's will present themselves as non-linear functions of the J's. To reverse this relationship, we use a trial and error method, similar to the Newton method used to find the zeros of one-dimensional functions.

The J's and the α's can be considered as vectors, denoted J and α respectively. A first estimate of J can be used to calculate α in order to compare it to its experimental value α_e. At the same stage, the matrix A of the partial derivatives $\frac{\partial \alpha_i}{\partial J_j}$ is also calculated. The J increment J_{new}-J_{old} is obtained by solving the linear system $\alpha_e - \alpha = A\,(J_{new}$-$J_{old})$ and the process is iterated until it converges.

5.3 ERROR PROPAGATION. — The error propagation is given by a local linearization of the relationship between the J's and the a's, which is summarized by the A^{-1} matrix : the error for the effective interaction J_i is given by

$$dJ_i = \sqrt{\sum_{j=1}^{R} (A_{ij}^{-1}\,\delta\alpha_j)^2}$$

The A^{-1} matrix can be diagonalized. Assuming identical error bars on the α's (spherical error volume), the eigenvector associated with the smallest eigenvalue points towards the direction of the most accurately determined combination of the interactions, the direction of the loosely determined combination being associated with the strongest eigenvalue. We measure the conditioning by the ratio C of the maximal to minimal eigenvalues. If C is strong, the system is badly conditioned, i.e. the errors on all interactions will be substantial, except for some linear combination of them. This situation is independent of the experimental data : it reflects only the local behaviour of the relationship between the J's and the α's.

5.4 RESULTS AND COMMENTS. — As, in our case, the CVM can yield interactions up to the fourth neighbour only, we used only four short-range order parameters.

Table VI displays the values found for the interactions obtained, their errors and the C parameters, together with the antiphase energy $\xi = J_2 - 4J_3 + 4J_4$ which, for the A_3B composition, is proportional to the energy needed to shift one half of the crystal by a $\langle 1/2\ 1/2\ 0 \rangle$ vector located in the (100) separating plane. This energy is relevant because, in a

Table VI. — *Effective interactions obtained by inverse* CVM *from the short range order parameters displayed in table IV. The combination* $\xi = J_2 - 4J_3 + 4J_4$ *is also displayed (Units :* meV) ; *same notation of error bars as in table IV. The* C *ratio is a measure of the conditioning.*

	Pd_3V (840 °C)	Ni_3V (1 100 °C)	Ni_2V (955 °C)	Ni_2V (975 °C)	Ni_2V (1 070 °C)	Ni_2V (1 140 °C)	Ni_3Cr (560 °C)	Ni_3Cr (720 °C)	Ni_2Cr (650 °C)	Ni_2Cr (800 °C)
J_1 (011)	45	35(3)	24(5) 16(3)	25(6) 17(3)	24(3) 17(2)	26(6) 19(3)	10.3(6)	10.9(2)	12.9(5)	12.5(7)
J_2 (002)	− 1.4	− 12(2)	− 21(4) − 18(7)	− 17(4) − 15(7)	− 15(2) − 13(3)	− 9(5) − 9(6)	− 6.2(3)	− 5.5(2)	− 3.0(5)	− 2.8(6)
J_3 (112)	5.7	− 3(2)	− 1(2) − 2.4(1.5)	0(3) − 2(2)	− 1(1) − 2(1)	0(3) − 1(2)	− 1.5(3)	− 1.1(2)	0.4(2)	1.0(3)
J_4 (022)	6.6	4(1)	12(3) 8(5)	11(4) 8(5)	9(2) 6(2)	8(4) 5(4)	4.3(2)	4.0(1)	2.8(3)	2.4(4)
ξ	2.4(3)	16(5)	31(5) 25(5)	27(5) 24(5)	25(5) 20(5)	23(5) 18(5)	7(5)	15(5)	7(3)	3(3)
C	100	30	13	15	13	13	5	3	9	7

model limited to four interactions, it is the energy difference per atom between the $L1_2$ and DO_{22} ordered states and also because, in the Bragg-Williams approximation, the short-range order maxima are located at 1/12 0 or 100 points if ξ is positive or negative.

The deviations of α_0 from unity (Sect. 4.7) must be taken into account : if they arise from a bad estimate of the incoherent scattering, the error is additive and the α's must be used without correction ; if they are due to errors in the sample size or in the absorption coefficient, the α's must be corrected by multiplying the α s by the ratio of the expected average intensity $\sigma^{inc} + \sigma^{MS} + 1$ to its experimental value. For Ni_2Cr and Ni_3V, this ratio is close to unity, the two procedures yield nearly the same interactions and we give only one result. For Ni_3Cr, a volume error is highly probable, and we give only the set of interactions deduced from the corrected α's. For Ni_2V, we give both sets of interactions calculated with the corrected and non-corrected α's : the truth should lie between the two results.

The antiphase energy is positive for all the alloys studied. This is consistent with the stability of DO_{22} at the A_3B composition. These positive values are not driven by the J_2, which are generally negative, but rather by a positive J_4 or a negative J_3. From the electronic structure standpoint, J_4 (indices 022) can be expected to be stronger than J_2 and J_3, because it involves two aligned 011 first neighbour jumps.

For Pd_3V, except for the antiphase energy ξ, the error bars are very large. This is due to the very large value of C, which is correlated with the low value of ξ. Indeed, with the set of interactions found experimentally, the system, at low temperatures, hesitates between two ordered structures which have nearly the same energy, but very different values of the α's. If this remains true in the disordered state, small variations of the interactions should induce large variations of the order parameters. Thus, for given error bars on the α s, we obtain a very accurate determination of ξ. The opposite situation will prevail if, in the space spanned by the four J interactions, we move into planes for which ξ is constant. In this case, the α s will hardly be modified. Hence, for given error bars on the α's the related

individual interactions will be loosely determined. The eigenvalue of A^{-1} in the ξ direction is small and the other eigenvalues are large : a large C ratio is expected.

Except for Ni_3V and Pd_3V, for which we lack information, the thermal variation of the interactions remain within the error bars : this implies that our experimental procedure is sound, and that the short-range order physics is well described by our truncated interaction model. However, a small systematic increase of J_2 with increasing temperature shows up for Ni_2V.

Whereas the interactions should be temperature independent, because the electronic structure is not sensitive to the temperature, they are expected to change with the concentration, which drives the electron per atom ratio. It is the case for the Ni-Cr system, as shown in figure 8, where we have plotted, as a function of the Cr concentration, the interactions found for our alloys together with the results of experiments performed by other authors on quenched samples containing 11 and 20 at.% Cr [11], [12]. Large discrepancies between our results and those of other authors would have led us to doubt of either set of results : it is not so, though significant variations are obvious.

Similarly, except for J_4, the interactions decrease, in absolute value, from Ni_3V to Ni_2V, in qualitative agreement with the decrease of the transition temperature. No previous experimental results were available for the Ni-V system, probably because of the impossibility to quench the disordered state in a whole range of concentrations.

The interaction J_1 between first neighbours is found to decrease from Ni_3V to Ni_3Cr. From Ni_2V to Ni_2Cr, it increases : these points will be discussed later on.

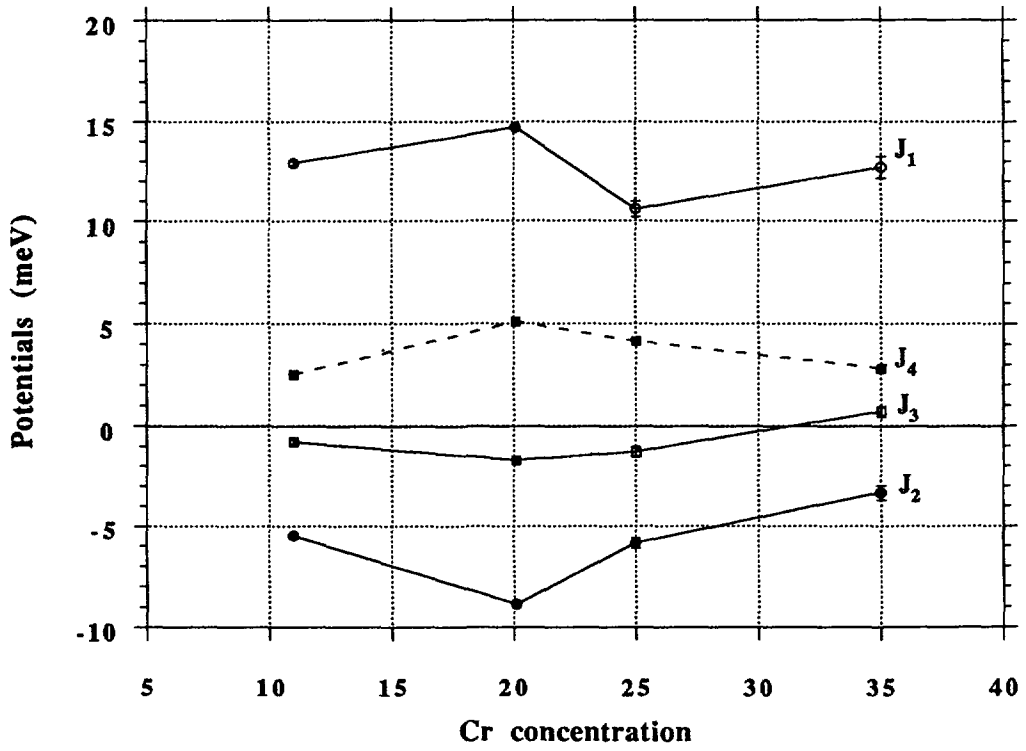

Fig. 8. — Comparison, for the Ni-Cr system, of our interatomic pair interactions (25 and 33 % Cr), with the values found by other authors for 11 % [10] and 20 % [11].

6. Discussion.

We first discuss the specific case of the 100 locations of the diffuse scattering for Pd_3V. Then we compare the interactions we have measured with the available electronic structure calculations. In the present state of the calculations, we can only expect qualitative comparisons, i.e. trends and orders of magnitude. In a second step, we submit our results to a more stringent test : we introduce them into models of statistical physics, and the predictions of these models are compared with other types of experimental results, such as phase stability and transition temperatures.

6.1 Pd_3V : BREAKDOWN OF THE MEAN FIELD APPROXIMATION. — First, let us briefly discuss the case of Pd_3V and its comparison with Ni_3V, which has already been explained elsewhere [26]. In a 2-interaction model (J_1 and J_2), the DO_{22} structure, which is the ground state of both alloys, is stabilized for $J_1 > 0$ and $0 < J_2/J_1 < 1/2$, whereas $L1_2$ would be stabilized for $J_2 < 0$. In the mean-field approximation, the regime of $J_2 > 0$ corresponds to diffuse intensity maxima located at 1 1/2 0 positions, whereas the regime of $J_2 < 0$ leads to maxima located at 1 0 0 [27] : the mean-field theory leads to a correct prediction for Ni_3V, but not for Pd_3V. To explain this discrepancy, we first performed CVM calculations, in the tetrahedron-octahedron (T.O.) approximation, including the effective interactions J_1 and J_2. The resulting phase diagram shows a narrow region ($J_2/J_1 < 0.08$), where the DO_{22} structure disorders towards a short range ordered FCC phase with diffuse maxima located at the 100 positions-100 regime, corresponding to the Pd_3V situation, whereas the Ni_3V pertains to the 1 1/2 0 regime ($J_2/J_1 > 0.08$) where the DO_{22} structure disorders towards a 1 1/2 0 disordered state. Provided that the first neighbour interaction is dominant, this phase diagram should remain qualitatively valid upon changing J_2 into the antiphase energy ξ. The values of ξ/J_1 are 0.05 for Pd_3V and 0.6 for Ni_3V : the critical value of 0.08, is in between, in agreement with the phase diagram we just mentioned, based on a J_1 and J_2 model, with J_2 replaced by ξ.

6.2. COMPARISON WITH THE ELECTRONIC STRUCTURE CALCULATIONS. — We first compare the trends suggested by our results with those calculated by the available models. This test is, to us, the most significant physically. We then try to compare the measured orders of magnitude with the calculated values.

6.2.1 *Trends.* — The concentration variation of the interactions for Pd-V and Ni-Cr systems has been calculated by the tight binding approximation (+ coherent potential approximation + generalized perturbation method [28], [29] or + DCA [30], which yields equivalent results), and the KKR approximation (also + CPA + GPM) [31], [32]. Thanks to the physical insight provided by the tight binding approximation, the concentration trends obtained by this method (but not the orders of magnitude) can be extended to Ni-V. For the same reasons, only this model can give access to the dependence of the effective interactions on the atomic species.

Figures 9 and 10, extracted from references [28] and [30] summarize, with some simple calculations added, the results obtained within the tight binding approximation on Pd-V like systems. They both show a decrease of J_1 with increasing vanadium concentration. This is consistent with our results on Ni-V. For Ni-Cr, only [28] gives information in the range we have studied. The calculated trend, i.e. a decrease from Ni_3Cr to Ni_2Cr, occurs to be opposite to the experimental one. This discrepancy can be explained by non-diagonal disorder, not taken into account, by the size effect, which is stronger for Ni-Cr than for Pd-V, or by an overestimated value of the diagonal disorder parameter $\delta = (\varepsilon_A - \varepsilon_B)/W$: indeed, a

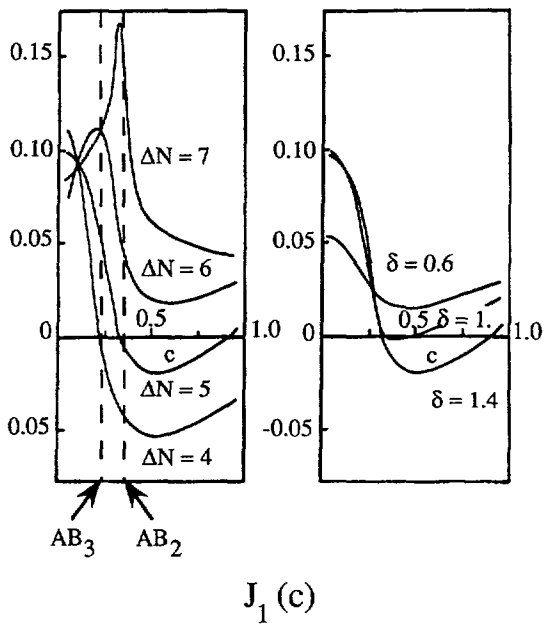

Fig. 9.

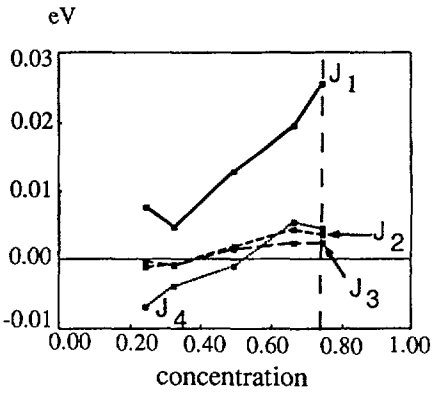

Fig. 10.

Fig. 9. — Interaction J_1 calculated by the TB/CPA/GPM approximation. J_1 is plotted as a function of the concentration c of the element A in B. The parameters are the electronic concentration N_B of the B element (which, for $N_B = 9$, is Ni or Pd) ; the difference ΔN of electronic concentration between B and A (if A is V or Cr, $\Delta N = 5$ or 4 respectively) and the difference δ of atomic energy levels between the two components, in units of the bandwidth [28]. The dashed vertical lines represent the alloys we have measured (arbitrary units).

Fig. 10. — Concentration variation of the interactions J_1, J_2, J_3 and J_4 calculated by the TB/Direct Configurational Averaging formalism [30]. Concentration 1 and 0 represent pure Pd or V, respectively. The dashed vertical line represents Pd_3V.

decrease of this parameter tends to shift the minimum of the J_1 curve for Cr towards the low vanadium concentrations. The general decrease of J_1 from the Ni-V to the Ni-Cr system is also correctly predicted by [32] although the decrease is far too strong. An overestimated δ can also account for this discrepancy.

For Pd_3V, the tight binding models predict an increase of the antiphase energy ξ with the vanadium concentration, which is consistent with the observation of a diffuse scattering located at 100 for 18 at.% V and at 1 1/2 0 for 29 % [6] (electron microscopy on quenched samples). The values of ξ are not accurate enough for Ni_3V and Ni_2V to extract a valid trend for the Ni-V system.

The KKR calculation performed on the Pd-V system [31] is doubtful as it predicts a decrease of ξ with the vanadium concentration. On the other hand, the trends of J_1 and ξ predicted by the KKR calculation performed on the Ni-Cr system are in agreement with the experiments, if the combined accuracy of our results and those of Schönfeld [12] is sufficient to extract experimental trends for ξ.

6.2.2 *Orders of magnitude.* — For Pd_3V, the only system for which tight binding calculations exist, the bad conditioning of the reversing procedure only enables us to establish a comparison for ξ, which is correctly predicted by both tight binding calculations [29], [30].

Using first neighbour jumps arguments the tight binding model is generally expected to yield, and indeed yields, J_2 much lower than J_1 (about 10 %) and J_4 a little bit stronger than J_2. The experimental results, and the KKR calculations yield values of J_2 hardly smaller, in absolute value, than J_1. May be this is due to the neglect, by the TB model, of direct paths between second neighbours, which should be important for J_2.

For the Ni-Cr system, the interactions J_2, J_3 and J_4 (hence ξ) calculated by KKR [32] are about twice the experimental values. The calculated J_1 is negative, which is unphysical, as it would lead to phase separation. The authors explain this discrepancy by charge transfer effects, or a high sensitivity to the Fermi energy. J_2 and J_4, considered as functions of the band filling, are nearly minimal. Hence, they are not too sensitive to the Fermi energy.

For Ni_3V, the antiphase energy has been calculated directly by comparing the energies of the DO_{22} and the $L1_2$ compounds, obtained by band structure calculations [33-35]. All the calculations yield $\xi \cong 100$ meV, which is much stronger than the experimental value. This discrepancy could be explained by the distortion included in the calculations for the ordered structures : these distortions are not present in the disordered phase, because of the cubic symmetry. However, these distortions are weak (1 % for Ni_3V, 2 % for Ni_2V). In reference [33], interactions calculated by the inversion method were used to build a phase diagram. These interactions are not displayed explicitly in the paper. We extracted them by inversion of a 7×7 linear system, and we obtained $J_1 \cong 40$ meV, which is in agreement with our results.

6.3 PREDICTIONS BASED ON THE MEASURED INTERACTIONS. — From the interactions we have obtained, two types of information can be deduced about the phase diagrams : the transition temperatures of the compounds we have studied and their phase stability.

6.3.1 *Phase stability.* — At zero temperature, the phase stability of a compound of concentration c results of the comparison of its energy E with the energy E_2 of a two-phase state, made of two neighbouring compounds, in such proportions that the average concentration is the same as the homogeneous compound. If the concentrations of the neighbouring compounds are c_L and c_R, and their energy E_L and E_R, the energy of the two-phase state can be written :

$$E_2 = \frac{c_R - c}{c_R - c_L} E_L + \frac{c - c_L}{c_R - c_L} E_R .$$

Similarly to (2), the energy of an ordered compound can be written :

$$E = \sum_{i=1}^{4} m_i x_i J_i ,$$

where J_i is the interaction for the i-th shell, m_i its multiplicity [36] and x_i its correlation function.

The multiplicities and pair correlation functions up to the ninth shell are given in table VII for the phases built on 1 1/2 0 concentration waves. Also shown are the correlation functions and multiplicities fot the linear triplet along the $\langle 110 \rangle$ direction.

As a first step, we assume the interactions to be concentration independent. $E - E_2$ can then be easily calculated as multilinear functions of the interactions : for the decomposition of Pt_2Mo into A_2B_2 and Au_5Mn_2 (see Tab. VII), in the framework of the four-interaction model, it depends only on J_2 and J_4 : $E - E_2 = -4/9(2J_2 + J_4)$.

For the decomposition of DO_{22} into Au_5Mn_2 and Ni_4Mo, the result is less simple : $E - E_2 = -1/3\, J_1 + 2/3\, J_2 - 2/3\, J_3 + 4/3\, J_4$.

Table VII. — *Multiplicities and correlation functions for some ordered compounds based on* 1 1/2 0 *concentrations waves.*

			20 %	25 %	28.6 %	33.3 %	50 %
Shell N°	Index	Mult.	Ni_4Mo	DO_{22}	Au_5Mn_2	Pt_2Mo	A_2B_2
1	011	6	1/5	0	− 1/21	− 1/9	− 1/3
2	002	3	7/15	2/3	3/7	1/9	1/3
3	112	12	7/15	1/3	1/3	1/3	1/3
4	022	6	1/5	1/3	1/21	− 1/9	− 1/3
5	013	12	1/3	0	1/21	1/9	− 1/3
6	222	4	1/5	0	− 1/7	1/3	− 1
7	123	24	7/15	1/3	2/7	− 1/9	1/3
8	004	3	7/15	1	3/7	1/9	1
9	033	6	1/5	0	1/7	1	− 1/3
T		6	− 1/5	− 1/6	− 1/3	− 7/9	0

Using the interactions measured for the compounds themselves, this simple analysis predicts the DO_{22} compounds Ni_3Cr, Ni_3V and Pd_3V to be stable, in agreement with the known phase diagrams, whereas Ni_2Cr and Ni_2V are not found stable, in contradiction with the experimental evidence. Taking into account the concentration variation of the interactions, by interpolation or extrapolation [38] does not change these conclusions : with the four interactions extracted from our data, the instability of the Pt_2Mo compounds remains to be explained.

6.3.2 *Transition temperatures.* — We have compared the experimental transition temperatures with the theoretical estimates obtained from our sets of interactions : by a Monte Carlo method, we obtain 600 °C for Pd_3V instead of 815 °C experimentally ; for Ni_3V, we obtain 985 °C instead of 1 045 °C and, for Ni_3Cr, the transition temperature is lower than 150 °C : all these results are consistent with the experimental situation. But, for the Pt_2Mo compounds, we find again strong discrepancies between the four-interaction model and the experiment : after a slight modification of the interactions in order to stabilize the ordered structures, the Monte Carlo simulation yields 350 K for the ordering temperature of Ni_2Cr instead of the experimental value of 850 K ; for Ni_2V, we find 340 K instead of 1 193 K. These results are still more puzzling than the instability of the compounds, which could be explained by strong concentration dependences of the interactions.

6.3.3 *Limitations of the four-interaction model.* — The transition temperatures of the Pt_2Mo compounds and their stabilities are not correctly predicted by the four-interaction model,

although Monte Carlo estimates of the diffuse intensity are in good agreement with the experimental maps. We must conclude that this limited range model describes the disordered state correctly, but fails to account for the energy of the long-range order state and, consequently, for its stability and its transition temperature. This can happen if we have neglected some interactions which are important for the Pt_2Mo structure, but not for the short-range order state. A look at table VII convinces us that this is indeed the case for the ninth neighbour (330), the coordination function of which is unity. This situation occurs for other shells of other structures, but what is specific to Pt_2Mo is that the multiplicity for the ninth shell is larger, and that the ninth neighbours can be reached by three collinear nearest neighbour jumps, which is important from the electronic structure viewpoint. However, to account for the whole discrepancy between the four-interaction model and the experiment, the ninth shell interaction should amount to some -4 meV, for Ni_2Cr, and -6 for Ni_2V which seems unrealistic, compared to the -1 meV order of magnitude found by Schweika *et al.* [11] for $Ni_{0.89}Cr_{0.11}$ and by Schönfeld *et al.* [12] for $Ni_{0.80}Cr_{0.20}$. We suspect another interaction to be important, namely the one which corresponds to the linear triplet along the ⟨110⟩ direction. This triplet should also be favoured by tight binding arguments, as it can be described by first collinear neighbour jumps [39].

7. Conclusions.

We have presented a rather complete experimental panel of effective pair interactions for several transition metal alloys. For a given system, we have estimated the concentration dependence of the interactions and, at constant concentration, the effect of the nature of the alloy components has been evaluated. A wealth of experimental data now exists, which enables us to test theoretical work.

The trends predicted by the tight binding-based calculations fit reasonably with the experimental results, except for the comparison between Ni_3Cr and Ni_2Cr. The concentration trends obtained by the KKR-based calculations are in agreement with the experiment for the Ni-Cr system, but in conflict for the Pd-V system. However, to obtain a more detailed comparison, the existing theories must be adapted to the very cases we have studied : for instance, band width and size effect variations must be taken into account to follow the effects on the Ni-V and Ni-Cr systems. Some steps are presently made in this direction.

Predictions have been deduced from our results. For the DO_{22} structure, the phase stability and the transition temperatures are in agreement with the experimental situation. On the other hand, the role of the ninth neighbour interaction (330) has been shown to be crucial for the specific case of the Pt_2Mo structure. Simple tight binding arguments suggest that this interaction can be sizeable. We also suspect other interactions, such as the triplet in the ⟨110⟩ direction, to be important for this structure. The diffuse scattering is not very sensitive to these interactions, but we are currently trying to extract them from our data by an inverse Monte Carlo method.

Acknowledgements.

The authors would like to thank B. Beuneu and P. Barberis for the development of the new software of the spectrometer, and also J. P. Ambroise and D. Regen for their efficient technical help.

References

[1] DUCASTELLE F., Alloy Phase Stability, G. M. Stocks and A. Gonis Eds., Nato ASI series, series E : Applied Sciences **163** (Kluwer Acad. Publ., 1989) p. 293.

[2] DUCASTELLE F., Order and Phase Stability in alloys, F. R. De Boer and D. G. Pettifor Eds., series cohesion and structure **3** (North Holland, 1991).

[3] PIERRON-BOHNES V., CADEVILLE M. C., FINEL A. and SCHAERPF O., *J. Phys. I France* **1** (1991) 247.

[4] STANSBURY E. E., VASUDEVAN K. and LEI T. S., Microstructural Science, S. A. Shiels *et al.* Eds. **13** (Elsevier, Ohio, 1985) p. 197.

[5] MOFFATT W. G., The handbook of binary phase diagrams (Genium Publishing Corp., 1984).

[6] Technical report ONERA 13/1221M (1987).

[7] HIRABAYASHI M., KOIWA M., TANAKA K., TADAKI T., SABURI T., NENNO S. and NISHIYAMA H., *Trans. J.I.M.* **10** (1969) 366.

[8] KÖSTER W. and HAEHL W. D., *Z. Metallkunde* **49** (1958) 647.

[9] BACON G. E., Neutron Diffraction (Clarendon Press, Oxford, 1975).

[10] KOESTER L. and STEYERL A., Neutron Physics, Springer Tracts in Modern Physics (Springer Verlag, 1977) ;
KOESTER L., RAUCH H. and SEYMANN E., Atomic data and nuclear tables **49** (1991) 65.

[11] SCHWEIKA W. and HAUBOLD H. G., *Phys. Rev.* **B 37** (1988) 9240.

[12] SCHÖNFELD B., REINHARDT L. and KOSTORZ G., *Phys. Status Solidi* b **147** (1988) 457.

[13] VINTAYKIN Ye. Z. and LOSHMANOV A. A., *Fiz. met. metalloved* **27** (1967) 754.

[14] LOISEAU A., Private Communication.

[15] BEUNEU B., PRIEM T., DE NOVION C. H., LEFEBVRE S., CHEVRIER J. and CHRISTENSEN A. N., *J. Appl. Cryst.* **27** (1990) 497.

[16] SPARKS J. C. and BORIE B. in : Local Atomic Arrangements Studied by X-Ray Diffraction, J. B. Cohen and J. E. Hilliard Eds. (Gordon and Breach, 1966).

[17] BLECH I. A. and AVERBACH B. L., *Phys. Rev.* **137** (1965) A1113.

[18] The B value for vanadium is usually 0.57 Å^2 with a different meaning for $|q|$, i.e. $|q| = \sin\theta/\lambda$ instead of $4\pi \sin\theta/\lambda$.

[19] One RLU is equivalent to $2\pi/a$Å^{-1}, i.e. about 1.78 Å^{-1} for nickel alloys.

[20] DE NOVION C. H., in « L'ordre et le désordre dans les matériaux », F. Raynaud, N. Clément et J. J. Couderc Eds. (Les Éditions de Physique, Les Ulis, 1984).

[21] COWLEY J. M., *J. Appl. Phys.* **21** (1950) 24.

[22] SCHWARTZ L. H. and COHEN J. B., Diffraction from materials, Materials Science Series (Academic Press, 1977).

[23] LAWSON C. L. and HANSON R. J., Solving Linear Least Squares Problem (Prentice-Hall, Englewood-Cliffs, New-Jersey, 1974).

[24] KIKUCHI R., *Phys. Rev.* **81** (1951) 988.

[25] SANCHEZ J. M., DUCASTELLE F., GRATIAS D., *Physica* **A 128** (1984) 334 ;
FINEL A., Thèse, Univ. Paris VI (1987).

[26] SOLAL F., CAUDRON R., DUCASTELLE F., FINEL A. and LOISEAU A., *Phys. Rev. Lett.* **58** (1987) 2245 ;
SOLAL F., CAUDRON R. and FINEL A., Alloy phase Stability, G. M. Stocks and A. Gonis Eds., Nato ASI series, series E : applied Sciences **163** (Kluwer Acad. Publ., 1989) p. 107.

[27] CLAPP P. C. and MOSS S. C., *Phys. Rev.* **171** (1968) 754.

[28] TURCHI P.,SLUITER M. and DE FONTAINE D., *Phys. Rev.* **B 36** (1987) 3161.

[29] BIEBER A., DUCASTELLE F., GAUTIER F., TREGLIA G. and TURCHI P., *Solid State Commun.* **45** (1983) 585 ;
BIEBER A. and GAUTIER F., *Acta Metall.* **34** (1986) 2291.

[30] WOLVERTON C., ASTA M., DREYSSÉ H. and DE FONTAINE D., *Phys. Rev.* **B 44** (1991) 4914.

[31] TURCHI P. E. A., STOCKS G. M., BUTLER W. H., NICHOLSON D. M. and GONIS A., *Phys. Rev.* **B 37** (1988) 5982.

[32] TURCHI P. E. A., PINSKI F. J., HOWELL R. H., WACHS A. L., FLUSS M. J., JOHNSON D. D., STOCKS G. M., NICHOLSON D. M. and SCHWEIKA W., *Mat. Res. Soc. Symp. Proc.* **166** (1990) 231.

[33] MIKALOPAS J., TURCHI P. E. A., SLUITER M. and STERNE P. A., unpublished (1990).

[34] PEI S., MASSALSKI T. B., TEMMERMANN W. M., STERNE P. A. and STOCKS G. M., *Phys. Rev.* **B 39** (1989) 5767.

[35] XU J. H., OGUCHI T. and FREEMAN A. J., *Phys. Rev.* **B 35** (1987) 6940.

[36] The multiplicity is defined as the coordination number divided by 2 for the pairs, by 3 for the triplets.

[37] The DO_{22} compound does not show up in the Ni-Cr diagram. This might be due to either a two-phase equilibrium state, or a too low transition temperature : in both cases, the thermodynamical equilibrium cannot be reached because of the diffusion sluggishness.

[38] The extrapolation towards the A_2B_2 composition is very pessimistic, because it amplifies considerably the errors on the 25 and 33 % concentrations.

[39] BIEBER A. and Gautier F., *Z. Phys.* **B 57** (1984) 335 ; *J. Phys. Soc. Jpn.* **53** (1984) 2061.